ELSEVIER

Global and Planetary Change 19 (1998) 3–18

GLOBAL AND PLANETARY CHANGE

The BASE land surface model

Carl E. Desborough *, Andrew J. Pitman

School of Earth Sciences, Macquarie University, North Ryde, NSW, 2109 Australia

Received 10 September 1997; accepted 9 February 1998

Abstract

The Best Approximation of Surface Exchanges (BASE) land surface model is described in detail. BASE is designed for large-scale climate modelling and for investigation of inter-model parameterisation differences. It has a tiled surface structure with an explicit canopy layer through which the foliage, underlying ground and atmosphere interact. A three-layer diffusion scheme is used to model soil temperature, moisture and ice content. A slab model is used to represent snow.

Keywords: numerical models; climate; atmosphere; hydrology; bisophere

1. Introduction

General circulation models (GCMs) require a description of land–atmosphere energy exchanges as a lower boundary condition and this is the principal function of a land surface model (LSM). LSMs can also be used to provide additional surface information such as temperature, humidity, soil wetness, snow-cover and runoff. Land surface modelling has been heavily influenced by the work of Manabe (1969) and Deardorff (1978). By incorporating the simple 'bucket' model of Budyko (1956) in the GFDL GCM, Manabe was the first to include an explicit representation of land surface hydrology in a GCM. Drawing on micrometeorological principles (e.g., Monteith, 1965), Deardorff proposed a more detailed representation of the land surface based around the diurnal-scale surface energy balance and the influence of vegetation on surface–atmosphere interactions.

The work of Deardorff led to the creation of more complex LSMs such as the Biosphere-Atmosphere Transfer Scheme (BATS: Dickinson et al., 1986) and the Simple Biosphere (SiB) model (Sellers et al., 1986). The Bare Essentials of Surface Transfer (BEST; Cogley et al., 1990; Pitman et al., 1991; Pitman and Desborough, 1996), Canadian LAnd Surface Scheme (CLASS; Verseghy, 1991; Verseghy et al., 1993), Goddard Institute for Space Studies (GISS; Abramopoulos et al., 1988), land-surface-transfer scheme (LSX; Bonan, 1994; Pollard and Thompson, 1995), LSM (Bonan, 1996) and BASE models are structurally and philosophically similar to BATS and SiB. Several LSMs have been constructed from

* Corresponding author. E-mail: cdesboro@penman.es.mq.edu.au

0921-8181/98/$ - see front matter
PII: S0921-8181(98)00038-1

Deardorff's philosophy but with an emphasis on simplification, e.g., Simple SiB (SSiB; Xue et al., 1991), Interactions between Soil Biosphere Atmosphere (ISBA; Noilhan and Planton, 1989; Mahfouf et al., 1995), Commonwealth Scientific and Industrial Research Organisation (CSIRO; Kowalczyk et al., 1991), Coupled Atmosphere Plant Snow (CAPS; Kim and Ek, 1995), Schématisation des Echanges Hydriques à l'Interface entre la Biosphère et l'Atmosphère (SECHIBA; Ducoudre et al., 1993) and European Centre for Medium-range Weather Forecasts (ECMWF; Viterbo and Beljaars, 1995).

The Project for Intercomparison of Land-surface Parameterization Schemes (PILPS) was initiated to assess the state of land surface modelling. Reviews of PILPS are given by Henderson-Sellers et al. (1993, 1995, 1996) and Pitman and Henderson-Sellers (1998). Intercomparison of LSM simulations in PILPS has revealed that the models do not behave in a consistent fashion. The division of incident radiation between land–atmosphere energy fluxes and the division of precipitation between evaporation and runoff has been shown to vary widely between LSMs at annual, seasonal and diurnal time-scales. Thus, there is a need to investigate the sources of these inconsistencies between LSMs.

The Best Approximation of Surface Exchange (BASE) LSM is designed principally as an experimental tool, providing a framework within which aspects of land surface modelling can be investigated. As such, BASE is not presented as the 'ultimate LSM' and other considerations have influenced its development. BASE is intended to be as 'typical' as possible, so that results are likely to have meaning for other models. It is designed to be inclusive so that it can be used to represent the range of parameterisations used in LSMs. BASE has a modular design with surface tiles treated as discrete elements in the code. Ground temperature and moisture calculations are performed separately. Snow calculations are separated from soil calculations. The coding of BASE also incorporates easily-replaced function calls. Another consideration in BASE's development was a desire to move towards simplicity where possible and this principle has been used where it does not impose on the other design principles.

BASE uses the modelling approach of Deardorff (1978) and is similar in design and complexity to two other Deardorff-type schemes: BATS and BEST. BASE was developed starting from the theoretical description of BEST given by Cogley et al. (1990) and many of its parameterisations follow from those of BEST. BASE differs from BEST in a number of ways. Its surface parameterisation is constructed around a tile structure that extends 10 cm into the soil. Each tile can have either the default canopy air space structure with separate foliage, ground and snow temperatures or an isothermal canopy structure. BASE has an explicit single-layer snowpack, whereas BEST combined snow with soil layers. The snowpack in BASE is modelled as a single layer on top of the soil column with energy and mass balances calculated for its upper and lower boundaries. Its temperature may differ from that of the surface soil layer. BASE has three soil moisture layers in place of BEST's two and BASE uses the same three layers for soil moisture and energy storage. BASE has a new set of soil hydraulic parameters developed from Cosby et al. (1984) and Patterson (1990) and includes simpler parameterisations for thermal conductivity and canopy resistance than BEST. BASE uses a new GCM interface developed by Hess and McAvaney (1997).

BASE is a full GCM LSM that can be applied to the whole of the global land surface. It has been implemented in the Australian Bureau of Meteorology Research Centre's (BMRC) GCM (McAvaney et al., 1991; McAvaney and Colman, 1993) and limited area model (LAPS; Timbal and Henderson-Sellers, 1998) and in the NCAR CCM3 model (Acker et al., 1996). BASE has participated in Phases 1c (Koster and Milly, 1997; Pitman et al., 1998), 2a (Chen et al., 1997), 2c, 2d, 3, 4a and 4b of PILPS. Its frozen soil moisture (Slater et al., 1998a) and snow (Slater et al., 1998b) parameterisations have been validated against observations from the former Soviet Union.

A detailed description of the BASE model is presented in this paper. Above- and below-ground parameterisation details are given in Sections 2 and 3, respectively. Parameter values are discussed in Section 4. Partial descriptions of BASE are given for hydrology by Desborough (1997), frozen soil moisture by Slater et al. (1998a) and snow by Slater et al. (1998b). A full list of the symbols used throughout this paper is given in Appendix A along with their meanings and units.

2. Surface parameterisation

BASE is constructed around a tiled surface structure (e.g., Koster and Suarez, 1992) with surface elements and fluxes expressed relative to a particular tile rather than to the whole surface (Fig. 1). The surface is divided into a number of canopy tiles and a single bare soil tile. Each canopy tile extends from the top of the canopy to the bottom of the 10 cm upper soil layer. The bare soil surface tile extends from the top of any snow that it is present to the bottom of the upper soil layer. Each tile is assigned a fractional extent (f_c, $m^2\ m^{-2}$), and all surface calculations are performed with respect to that fractional area rather than to the whole surface. Energy and moisture fluxes are expressed in W m^{-2} and kg m^{-2} s^{-1}, respectively, where 'm^{-2}' refers to the area of the tile rather than the whole surface. Portions of each tile's surface area can be shaded by foliage (A_f, $m^2\ m^{-2}$) and/or covered by snow (A_n, $m^2\ m^{-2}$).

Currently, the interface between BASE and the BMRC GCM has not been modified to make use of BASE's tile structure, and information exchanged between the two models has to be filtered to account for this incompatibility. The PILPS Phase 1 and 2 experiments are also designed for a single-canopy surface structure. The GCM filtering procedure that makes BASE emulate a single-canopy model is used for BASE's PILPS simulations and for the experiments in this thesis.

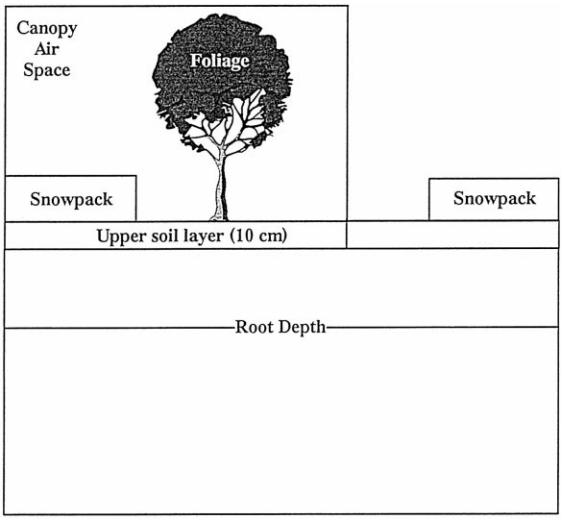

Fig. 1. Schematic representation of BASE's surface structure.

Sections 2.1 and 2.2 describe the procedures used to resolve the moisture and energy balances of each surface tile, while Section 2.3 describes how the tiles are combined to present a single land–atmosphere interface to the atmosphere.

2.1. Moisture balance of a surface tile

Moisture enters the surface system as either rain (P_r) or snow (P_n) depending on temperatures supplied by the host model. In off-line simulations, a 0°C snow–rain criteria is applied to near-surface air temperature (T_a). Rain falls evenly across the grid-square and is divided between the various interception surfaces in proportion to their areal extents.

Rain intercepted by the foliage collects in a foliage interception bucket (W_f, kg m^{-2}) until the bucket's capacity ($W_{f.max}$) is reached and any further rain falls through to the underlying ground (Y_{fg}). The prognostic foliage moisture storage variable (W_f) is updated according to:

$$dW_f/dt = A_f P_r - Y_{fg} - E_{fc} \quad (1)$$

where E_{fc} is the evaporation flux from W_f to the canopy air space; A_f is the tile's foliage fraction. BASE's foliage moisture balance is illustrated in Fig. 2a.

All snowfall (P_n) is added directly to the snowpack moisture store. The prognostic snow mass variable (W_n, kg m^{-2}) is updated according to:

$$W_n = P_n - E_{nc} - Y_{ng} \quad (2)$$

where E_{nc} is the flux of water vapour from the snowpack to the canopy air space and Y_{ng} is snowmelt runoff (Section 2.2). Rain intercepted by the snowpack is immediately available for infiltration. The melting of snow by rain is not represented in BASE. The snowpack moisture balance is illustrated in Fig. 3a.

All moisture reaching the soil surface is lumped together and divided between infiltration (I) and surface runoff (Y_s) according to:

$$I = \min\left(A_{dry} I^* (1 - A_f) P_r + Y_{fg} + Y_{ng}\right) \quad (3)$$

$$Y_s = \left[(1 - A_f) P_r + P_{r,fg} + Y_{ng}\right] - I \quad (4)$$

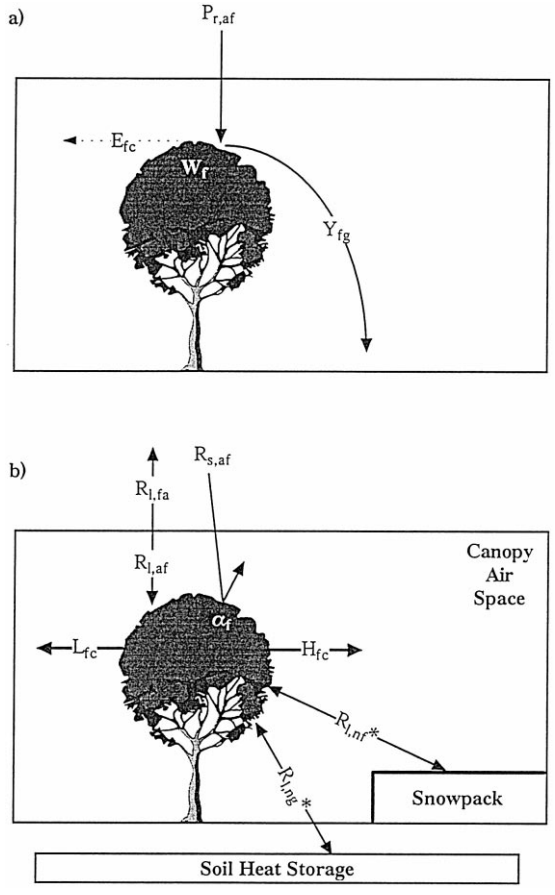

Fig. 2. Schematic representation of BASE's moisture (top panel) and energy balances (lower panel) for the foliage. The fluxes and state variables are described in the text.

The maximum infiltration rate ($A_{dry} I^*$) is discussed in Section 3.1.

Each surface tile can contain up to four evaporating surfaces, and all vapour exchanges between these surfaces and into the atmosphere occur through the canopy air space (CAS). Moisture stored on the foliage evaporates (E_{fc}) at the potential rate:

$$E_{fc} = A_f f_{wet} \rho_a (q_f^* - q_c)/r_{a.f} \quad (5)$$

where q is specific humidity ($m^3\ m^{-3}$) and the subscripts f and c refer to the foliage and canopy air space, respectively; ρ_a is the density of air ($kg\ m^{-3}$). Transpiration (E_{tr}) can occur from any dry foliage and is limited by wet stomatal resistance (r_c^*; Section 4.1.4) and by the maximum extraction rate ($E_{tr.sup}$):

$$E_{tr} = \min\left[A_f (1 - f_{wet}) \rho_a (q_f^* - q_c) / (r_{a.f} + r_c^*) E_{tr.sup} \right] \quad (6)$$

Evaporation from snow-free ground is limited by its maximum supply rate ($E_{gc.sup}$):

$$E_{gc} = \min\left[(1 - A_n) \rho_a (q_g^* - q_c)/r_{a.g} E_{gc.sup} \right] \quad (7)$$

The vapour flux from the snowpack (E_{nc}) is given by:

$$E_{nc} = A_n \rho_a (q_n^* - q_c)/r_{a.g} \quad (8)$$

Fluxes from the foliage (E_{fc} and E_{tr}) and ground (E_{gc} and E_{nc}) must overcome their respective aerodynamic resistances ($r_{a.f}$ and $r_{a.g}$; Section 4.1.3).

Evaporation fluxes are evaluated as part of their respective energy balances (Section 2.2). The humid-

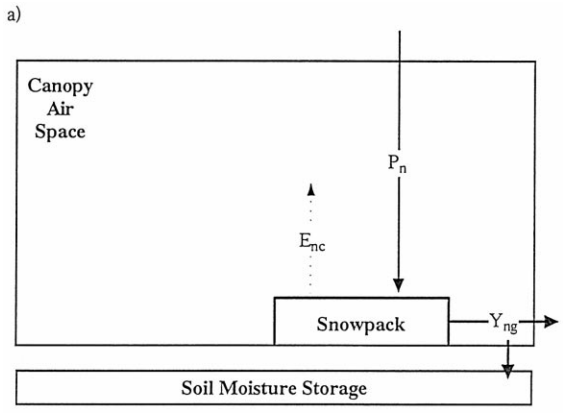

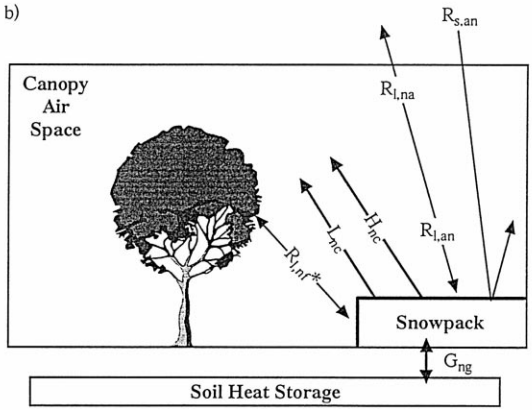

Fig. 3. Schematic representation of BASE's moisture (top panel) and energy balances (lower panel) for the snowpack. The fluxes and state variables are described in the text.

ity change in the CAS is assumed to be negligible and mass continuity is used to obtain the total evaporation flux for the tile:

$$E_{ca} = E_{fc} + E_{tr} + E_{gc} + E_{nc} \quad (9)$$

Finally, the humidity in the CAS (q_c) is updated by combining equations (5)–(9) with:

$$E_{ca} = \rho_a (q_c - q_a)/r_a \quad (10)$$

and solving for q_c. Evaporation fluxes are not recalculated with this new value of q_c. It is used to evaluate evaporation fluxes in the next timestep.

The maximum supply rate for E_{tr} is parameterised following Cogley et al. (1990) as:

$$E_{tr.sup} = A_f [1.8 \times 10^{-4}] S \times \sum_i \left\{ R_i \left(1 - \min\left[1.\Psi_i/\Psi_{wp}\right]\right)\right\} \quad (11)$$

S is a quadratic seasonality factor varying from one at 25°C to zero at 0 and 50°C. The moisture availability function is calculated as a root-weighted average (R_i is the fraction of roots in layer i) and depends on the actual soil moisture potential (Ψ_i) and its value at wilting point (Ψ_{wp}). The maximum transpiration rate is set to 1.8×10^{-4} kg m^{-2} s^{-1}. The supply function for soil evaporation ($E_{g.sup}$) is modelled as the inverse process to infiltration and uses a similar parameterisation. The formulation and its derivation are given by Cogley et al. (1990) and Pitman et al. (1991).

2.2. Energy balance of a surface tile

The foliage, snowpack and surface soil layer each have their own temperature and a separate energy balance equation is developed for each of these surfaces. After dividing incoming radiation between the surfaces, their energy balances are resolved in sequence: foliage, snow and surface soil layer. Finally, the total fluxes from the top of the CAS are calculated and the temperature of the CAS (T_c) is updated.

Incoming shortwave radiation ($R_{s.ac}$) is divided between surface elements based on foliage (A_f) and snow (A_n) cover fractions:

$$R_{s.af} = A_f R_{s.ac} \quad (12)$$

$$R_{s.ag} = (1 - A_f)(1 - A_n) R_{s.ac} \quad (13)$$

$$R_{s.an} = (1 - A_f) A_n R_{s.ac} \quad (14)$$

Incoming longwave radiation ($R_{l.ac}$) is split into $R_{l.af}$, $R_{l.ag}$ and $R_{l.an}$ components in a similar fashion. Unlike some other models (e.g., BATS, BEST, SiB), BASE makes no distinction between visible and near infrared components of the shortwave spectrum.

BASE's foliage energy balance is illustrated in Fig. 2b and can be written as:

$$0 = (1 - \alpha_f) R_{s.af} + R_{l.af} + R^*_{l.gf} + R^*_{l.nf} - H_{fc} - L_{fc} - R_{l.fa} \quad (15)$$

where:

$$H_{fc} = A_f \rho_a c_p (T_f - T_c)/r_{a.f} \quad (16)$$

$$L_{fc} = \lambda_v (E_{fc} + E_{tr}) \quad (17)$$

$$R_{l.fa} = A_f \sigma_{sb} T_f^4 \quad (18)$$

$$R^*_{l.gf} = A_f (1 - A_n) \sigma_{sb} \left(T_g^4 - T_f^4\right) \quad (19)$$

$$R^*_{l.nf} = A_f A_n \sigma_{sb} \left(T_n^4 - T_f^4\right) \quad (20)$$

The foliage reflects a fraction (α_f; Section 4.1.1) of $R_{s.af}$ and absorbs the rest. It exchanges longwave radiation with the atmosphere ($R_{l.af}$ and $R_{l.fa}$), ground ($R^*_{l.gf}$) and snowpack ($R^*_{l.nf}$). Sensible (H_{fc}) and latent (L_{fc}) heat are exchanged with the CAS. L_{fc} is related to the evaporative moisture flux by the latent heat of vaporisation (λ_v, J kg^{-1}). Change in foliage energy storage is assumed to be negligible. The foliage energy balance is solved for foliage temperature (T_f) using a combination of Newton's method and bisection. Careful consideration is given to ensure that the energy balance terms are monotonically non-increasing functions of T_f so that Eq. (15) will always have a solution and the bisection method will always converge.

BASE's snowpack energy balance is illustrated in Fig. 3b, and for subfreezing snow temperatures, it can be written as:

$$C_n dT_n/dt = \left[(1 - \alpha_n) R_{s.an} + R_{l.an} - R^*_{l.nf}\right] - H_{nc} - L_{nc} - R_{l.na} - G_{ng} \quad (21)$$

where:

$$H_{nc} = A_n \rho_a c_p (T_n - T_c)/r_{a.g} \quad (22)$$

$$L_{nc} = A_n \lambda_s E_{nc} \quad (23)$$

$$R_{l.na} = A_n \sigma_{sb} T_n^4 \quad (24)$$

The snowpack reflects a portion (α_n; Section 4.1.2) of the solar radiation that is incident upon it ($R_{s.an}$) and absorbs the remainder. It exchanges longwave radiation with the atmosphere ($R_{l.an}$ and $R_{l.na}$) and foliage ($R^*_{l.nf}$) and sensible (H_{nc}) and latent (L_{nc}) heat with the CAS. L_{nc} is related to the evaporative moisture flux by the latent heat of sublimation (λ_s, J kg^{-1}). Energy is also transferred across the snowpack's lower boundary (G_{ng}). The snowpack's heat capacity (C_n, J m^{-2} K^{-1}; Section 4.3) describes how its temperature (T_n) changes in response to a net input of energy. Eq. (21) is solved for T_n using Penman's q^* approximation (Penman, 1948) to remove the nonlinear T_n-dependence of L_{nc}. $R^*_{l.nf}$ has already been calculated as part of the foliage energy balance and its T_n-dependence is ignored for the purposes of updating T_n. The snowpack has a maximum temperature of 273.16 K and if the T_n calculated from Eq. (21) would exceed this value, the additional energy is used to melt some of the snow (Y_{ng}). The flux of heat from the centre of the snowpack to the centre of the surface soil layer (G_{ng}) is given by:

$$G_{ng} = A_n K_{T.ng}(T_n - T_g)/d_{ng} \tag{25}$$

where d_{ng} is the distance between the centres and $K_{T.ng}$ is the thermal conductivity for that path. $K_{T.ng}$ is calculated as a depth-weighted geometric mean of $K_{T.n}$ (Section 4.3) and $K_{T.g1}$ (Section 4.2.3).

The surface soil layer's energy balance is illustrated in Fig. 4 and can be written as:

$$\begin{aligned}(C_g d_1)\mathrm{d}T_g/\mathrm{d}t = \big[(1-\alpha_g)R_{s.ag} + R_{l.ag} - R^*_{l.gf} \\ - G_{12} + \lambda_f \Gamma_1 + G_{ng}\big] - H_{gc} \\ - L_{gc} - R_{l.ga}\end{aligned} \tag{26}$$

where:

$$H_{gc} = (1-A_n)\rho_a c_p (T_g - T_c)/r_{a.g} \tag{27}$$

$$L_{gc} = (1-A_n)\lambda_v E_{gc} \tag{28}$$

$$R_{l.ga} = (1-A_n)\sigma_{sb} T_n^4 \tag{29}$$

$$\begin{aligned}G_{12} = (1-A_n)\big[4(d_1 K_{T.1} + d_2 K_{T.2}) \\ \times (T_g - T_{g2})/(d_1 + d_2)^2\big]\end{aligned} \tag{30}$$

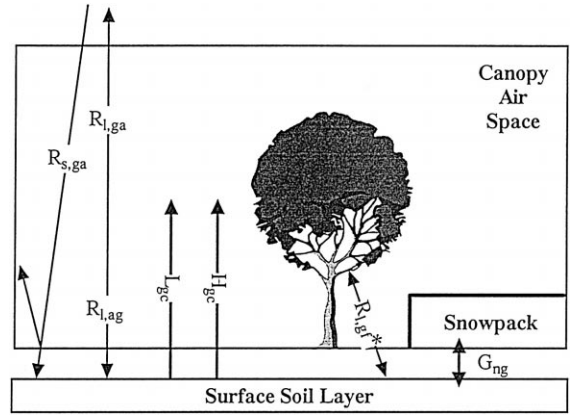

Fig. 4. Schematic representation of BASE's energy balance for the upper soil layer. The fluxes and state variables are described in the text.

The soil reflects a fraction (α_g) of incident solar radiation ($R_{s.ag}$) and exchanges longwave radiation with the atmosphere ($R_{l.ga}$ and $R_{l.ag}$) and foliage ($R^*_{l.gf}$). Sensible (H_{gc}) and latent (L_{gc}) heat are exchanged with the CAS. Energy is diffused down from the snowpack (G_{ng}) and down into the second soil layer (G_{12}, Section 3.2). Energy is released or absorbed (λ_f, 3.3×10^5 J kg^{-1}) by the layer's soil moisture when it changes between liquid and solid states (Γ_1). The soil's volumetric heat capacity (C_g, W m^{-3} K^{-1}) characterises its energy storage capability (Section 4.2.3). Eq. (26) is solved for the layer-average temperature (T_g) using an iterative bisection method in which the temperature-dependencies of H_{gc}, L_{gc} and $R_{l.ga}$ are considered. The bracketed terms on the right-hand-side of Eq. (26) either have no T_g-dependence or their T_g-dependence is not included in the iterative solution of the equation. T_g appears to be numerically stable for this solution procedure.

Changes in energy and moisture storage by the canopy air are considered to be negligible and total energy fluxes from the surface tile to the atmosphere can thus be obtained by summing the fluxes from each of the surface elements:

$$R_{s.ca} = \alpha_f R_{s.af} + \alpha_g R_{s.ag} + \alpha_n R_{s.an} \tag{31}$$

$$R_{l.ca} = R_{l.fa} + R_{l.ga} + R_{l.na} \tag{32}$$

$$H_{ca} = H_{fc} + H_{gc} + H_{nc} \tag{33}$$

$$L_{ca} = L_{fc} + L_{gc} + L_{nc} \tag{34}$$

After all the fluxes have been resolved, the canopy air temperature (T_c) is updated by combining an alternative expression for H_{ca}:

$$H_{ca} = \rho_a c_p (T_c - T_a)/r_a \quad (35)$$

with Eqs. (16), (22), (27) and (33). Sensible heat fluxes are not recalculated with the new value of T_c. It is used for energy balance calculations in the next timestep. This solution procedure appears to be numerically stable.

2.3. BASE's land–atmosphere interface

Despite dividing the surface into a number of discrete tiles for its internal calculations, BASE presents a single land–atmosphere interface to the atmosphere. The moisture and energy fluxes from each of BASE's surface tiles are area-weighted to provide the atmosphere with a single set of effective surface fluxes:

$$E_{sa} = \sum_i [A_i E_{ia}] \quad (36)$$

$$L_{sa} = \sum_i [A_i H_{ia}] \quad (37)$$

$$H_{sa} = \sum_i [A_i K_{l.ia}] \quad (38)$$

$$R_{l.sa} = \sum_i [A_i K_{l.ia}] \quad (39)$$

$$R_{s.sa} = \sum_i [A_i R_{s.ia}] \quad (40)$$

An effective surface radiating temperature (T_{rad}, K) is calculated from $R_{l.sa}$:

$$T_{rad} = (R_{l.sa}/\sigma_{sb})^{1/4} \quad (41)$$

Hess and McAvaney (1997) describe how effective surface state variables can be obtained from L_{sa} and H_{sa}. By calculating an aerodynamic transfer coefficient ($C_{H.sa}$) for the effective surface, they obtain values for its potential temperature (T_s), specific humidity (q_s) and wetness (β_s):

$$L_{sa} = \lambda_v C_{H.sa}(q_s - q_a) = \lambda_v C_{H.sa}\beta_s(q_s^* - q_a) \quad (42)$$

$$H_{sa} = \rho_a c_p C_{H.sa}(T_s - T_a) \quad (43)$$

Some constraints are required to avoid occasional nonphysical behaviour such as negative β_s (appropriate constraints for BASE are discussed by Hess and McAvaney, 1997).

3. Soil parameterisation

BASE models soil moisture and energy storage in three vertical layers and each layer has prognostic variables for temperature, liquid moisture content and frozen moisture content. The 10 cm surface soil layer is treated separately for each surface tile while the other two layers are common to all tiles. BASE's soil moisture and temperature parameterisations are described in Sections 3.1 and 3.2. Soil parameters are described in Section 4.2.

3.1. Soil moisture parameterisation

Water can exist in BASE's soil column as either a liquid or a solid (Fig. 5). Each of the three vertical layers has two prognostic variables to describe its liquid (θ_1, θ_2 and θ_3; $m^3\ m^{-3}$) and solid (θ_{i1}, θ_{i2} and θ_{i3}; $m^3\ m^{-3}$) volumetric moisture contents. Within BASE, these volume fractions are usually expressed as fractions of saturation, e.g., θ_1/θ^* where θ^* is porosity. Liquid moisture diffusion fluxes are calculated with respect to effective saturation fractions (V_1, V_2 and V_3) for which porosity is reduced to account for space taken up by frozen soil moisture.

The moisture balance equations for each of the prognostic soil moisture variables are:

$$d\theta_1/dt = I - Y_{12} - E_g - E_{tr.1} - \Gamma_1 \quad (44)$$

$$d\theta_2/dt = Y_{12} - Y_{23} - E_{tr.2} - \Gamma_2 \quad (45)$$

$$d\theta_3/dt = Y_{23} - Y_d - E_{tr.3} - \Gamma_3 \quad (46)$$

$$d\theta_{i1}/dt = \Gamma_1 \quad (47)$$

$$d\theta_{i2}/dt = \Gamma_2 \quad (48)$$

$$d\theta_{i3}/dt = \Gamma_3 \quad (49)$$

Liquid moisture enters the soil as infiltration (I), is exchanged between soil layers (Y_{12} and Y_{23}) and drains from the base of the soil column (Y_d). When moisture exists in an anomalous state with respect to its freezing point (273.16 K), mass is exchanged

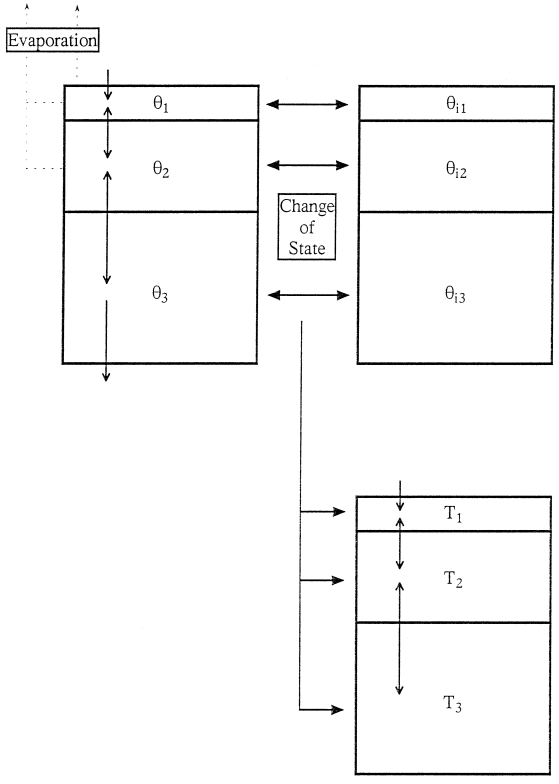

Fig. 5. Schematic representation of BASE's soil parameterisation showing liquid soil moisture (top left), frozen soil moisture (top right) and soil temperature (bottom). The fluxes and state variables are described in the text.

between the liquid and solid moisture stores in a layer (Γ_1, Γ_2 and Γ_3). Evaporation can occur at the soil surface (E_g) and vegetation can remove moisture ($E_{tr.1}$, $E_{tr.2}$ and $E_{tr.3}$) from within the root-zone. $E_{tr.3}$ is always equal to zero in the GCM, but may be non-zero if the root-zone extends down into the third layer as it does for PILPS Phase 2b. The moisture balance of the surface soil layer is resolved separately for each surface tile and the resulting Y_{12} fluxes are area-weighted to produce a single Y_{12} flux for use in Eq. (44).

Vertical diffusion of liquid soil moisture is parameterised in terms of Darcian motion where a flux of water (Y, kg m^{-2}) is related to the vertical moisture potential gradient ($\mathrm{d}\Psi/\mathrm{d}z$) by an effective hydraulic conductivity (K_H):

$$Y = \rho_w K_H \mathrm{d}\Psi/\mathrm{d}z \tag{50}$$

ρ_w is the density of water (1000 kg m^{-3}). Moisture potential (Ψ) in BASE has two additive components: gravitational and matric potential (Ψ_m). The depth-derivative of gravitational potential is unity and Eq. (50) thus becomes:

$$Y = \rho_w K_H (1 + \mathrm{d}\Psi_m/\mathrm{d}z) \tag{51}$$

Clapp and Hornberger (1978) give expressions for the moisture-dependence of K_H and Ψ_m:

$$K_H = K_H^* (\theta/\theta^*)^{2B+3} \tag{52}$$

$$\Psi_m = \Psi_m^* (\theta/\theta)^{-B} \tag{53}$$

Following Cogley et al. (1990), these expressions are applied to effective saturation fractions (V_{12} and V_{23}) at the layer boundaries to give Y_{12} and Y_{23}:

$$Y_{12} = \rho_w K_H^* V_{12}^{2B+3} \times \left[1 - B\Psi_m^* V_{12}^{-B-1}(V_1 - V_2) d_1\right] \tag{54}$$

$$Y_{23} = \rho_w K_H^* V_{23}^{2B+3} \times \left[1 - B\Psi_m^* V_{23}^{-B-1}(V_2 - V_3) d_2\right] \tag{55}$$

V_{12} and V_{23} are linearly interpolated between the centres of their respective layers using the depth of the layer above the boundary as a length scale. Soil hydraulic parameters (K_H^*, Ψ_m^*, θ^* and B) are parameterised following Clapp and Hornberger (1978) and Cosby et al. (1984) (Section 4.2.2).

Drainage out of the soil column is treated quite simply in BASE, being set to the gravitational drainage rate:

$$Y_d = \rho_w K_H^* V_3^{2B+3} \tag{56}$$

Water cannot move up into the soil column from below and no account is taken of water table depth or of slope.

Infiltration is parameterised following Cogley et al. (1990). A theoretical maximum infiltration rate (I^*) is calculated assuming horizontal homogeneity of near-surface soil moisture and a crude 'heterogeneity multiplier' (A_{dry}) is used to account for partial saturation of the surface:

$$I^* = \rho_w \left[K_H^* - \left(-4B\Psi_m^* K_H^* (\theta^* - \theta_{i1}) / \pi \Delta t\right)^{1/2}\right](V_1 - 1) \tag{57}$$

$$A_{dry} = 1 - \left[(\theta_1 + \theta_{i1})/\theta^*\right] \tag{58}$$

Δt is the timestep. The derivation of Eq. (57) is given by Cogley et al. (1990).

The melting and freezing of soil moisture is parameterised following Cogley et al. (1990) but because BASE uses the same layer structure for temperature and soil moisture layers, BEST's geometric factors are not required and the ice production rate for a layer (Γ_i) is simply:

$$\Gamma_i = \chi_i C_w (273.16 - T_i)/(\lambda_f \Delta t) \quad (59)$$

where χ_i is an 'efficiency factor', C_w is volumetric heat capacity of water (J m^{-3} K^{-1}), T_i is soil temperature (K), λ_f is water's latent heat of fusion (333 kJ kg^{-1}) and Δt is the timestep (s).

3.2. Soil temperature parameterisation

Storage of energy by the soil is parameterised in BASE with a three-layer finite-difference diffusion model and the three layers correspond to those used for moisture storage (Fig. 5). Vertical diffusion of heat within the soil (G, W m^{-2}) can be characterised by the thermal conductivity (K_T, J m^{-1} K^{-1}) of the soil (e.g., Hillel, 1980):

$$G = K_T \mathrm{d}T/\mathrm{d}z \quad (60)$$

In BASE, Eq. (60) is integrated over the path joining the centres of layers i and j to give the heat diffusion flux (G_{ij}) between the two layers:

$$G_{ij} = 4(d_i K_{T.i} + d_j K_{T.j})(T_{g.i} - T_{g.j})/(d_i + d_j)^2 \quad (61)$$

This equation is used to describe the diffusion fluxes between layers 1 and 2 (G_{12}) and layers 2 and 3 (G_{23}). A zero heat flux condition is imposed at the base of the soil column. BASE's parameterisation of K_T is given in Section 4.2.3.

The temperatures of BASE's two lower soil layers (T_{g2} and T_{g3}) change over time in response to heat diffusion from above and below and melting or freezing of soil moisture:

$$\mathrm{d}T_{g2}/\mathrm{d}t = 1/(C_g d_2)[G_{12} - G_{23} + \lambda_f \Gamma_2] \quad (62)$$

$$\mathrm{d}T_{g3}/\mathrm{d}t = 1/(C_g d_3)[G_{23} + \lambda_f \Gamma_3] \quad (63)$$

The soil's volumetric heat capacity (C_g, W m^{-3} K^{-1}) is a measure of how much its temperature will change in response to the net energy influx. BASE's C_g parameterisation is given in Section 4.2.3. Γ_2 and Γ_3 are the net mass of freezing moisture (kg m^{-2} s^{-1}) for layers 2 and 3, respectively (Section 3.1), and λ_f is water's latent heat of fusion (3.3×10^5 J kg^{-1}).

The temperature of the surface soil layer changes more rapidly than the other soil temperatures and, to avoid numerical instability, it is updated in an iteration with some of the fluxes that depend on it. The surface soil layer energy balance is resolved separately for each surface tile, producing a flux into the second soil layer:

$$G_{12.i} = 4(d_1 K_{T.1} + d_2 K_{T.2})(T_g - T_{g2})/(d_1 + d_2)^2 \quad (64)$$

and the resulting G_{12} fluxes are area-weighted to get a total G_{12} for use in Eq. (62).

$$G_{12} = \sum_i f_i G_{12.i} \quad (65)$$

4. Parameters

4.1. Surface parameters

4.1.1. Vegetation properties

Snow-free fractional foliage cover (f_f^*), leaf area index (Λ_L), stem area index (Λ_S), surface root fraction (R_1), root-zone depth (Z), foliage roughness length ($z_{0.f}$) and foliage albedo (α_f) are prescribed in BASE as functions of vegetation type. Effective vegetation properties are calculated for each gridsquare by averaging the properties of whatever vegetation is present. Fractional areas are calculated for each of the primary vegetation classes in the $1° \times 1°$ global vegetation map of Wilson and Henderson-Sellers (1985). Most of the gridsquare vegetation properties are then obtained by a linear area-weighted average across these fractional areas. An area-weighted log average is used for roughness length because it varies over several orders of magnitude. The averaging procedure is applied only to the vegetated portion of the gridsquare and the resulting properties apply to this fraction only.

Fractional foliage cover in the absence of snow (f_f^*) and leaf area index (Λ_L) vary seasonally with depth-weighted soil temperature (T_g^*):

$$f_f^* = f_{f.max} - (1 - S[T_g^*])\, f_{f.seas} \quad (66)$$

$$A_L = A_{L.max} - (1 - S[T_g^*])\, A_{L.seas} \quad (67)$$

$S[T]$ is a seasonality function (following BATS) that is equal to 0 for temperatures less than 0°C and to 1

for temperatures greater than 25°C with a quadratic transition between these two limits. Part of f_f^* can be covered by snow ($A_{n.f}$) and the actual foliage fraction (f_f) is given by:

$$f_f = (1 - A_{n.f}) f_f^* \quad (68)$$

BASE's vegetation snow-masking parameterisation is described in Section 4.3. The canopy in BASE extends beyond f_f and the canopy fraction (f_c) is given by:

$$f_c = f_f + f_f(1 - f_f) \quad (69)$$

This is a modified version of the self-similarity method employed in BEST. The foliage extent (A_f) for the canopy tile is then given by:

$$A_f = f_f / f_c \quad (70)$$

4.1.2. Albedo

Separate albedo values are specified for each surface type in BASE. Foliage albedo (α_f) is a seasonally invariant function of vegetation type. Soil albedo (α_g) depends on the soil colour index of Wilson and Henderson-Sellers (1985) and the moisture content in the surface soil layer (θ_1). The snowpack's albedo (α_n) is equal to 0.67 when its temperature (T_n) is 0°C and increases with decreasing T_n to a maximum value of 0.85 at −10°C. The effective albedo of a surface tile or of the whole surface is obtained by area-weighting the constituent albedo values.

4.1.3. Aerodynamic resistances

BASE's representation of aerodynamic resistances is constructed so as to be consistent with the aerodynamics of the BMRC GCM. The aerodynamic resistance (r_a) for heat and moisture fluxes from a surface tile to the atmospheric reference level (z_a) is calculated from the drag coefficient (C_{Dh}):

$$r_a = 1/(C_{Dh} u_a) \quad (71)$$

$$C_{Dh} = F_H \{k_{VK}/\log[(z_a + z_{0.c})/z_{0.c}]\}^{1/2} \quad (72)$$

where k_{VK} is the Von Karman constant (0.4). F_H depends on the static stability of the atmosphere and this dependence is parameterised in terms of the bulk Richardson number (R_{iB}).

The dependence of aerodynamic transport on the physical structure of the surface is characterised by roughness lengths. An effective roughness length ($z_{0.c}$) is calculated for each surface tile by averaging the roughness lengths of its constituent surfaces using a weighted geometric mean:

$$\log[z_{0.c}] = A_f \log[z_{0.f}] + (1 - A_f)\{A_n \log[z_{0.n}] + (1 - A_n)\log[z_{0.n}]\} \quad (73)$$

Foliage roughness length ($z_{0.f}$) is a seasonally invariant function of vegetation type, but $z_{0.c}$ varies seasonally with foliage fraction (A_f). The ground and snow surfaces have roughness lengths of 0.01 and 0.001 m, respectively.

Aerodynamic resistances for fluxes within the CAS are parameterised following BATS. The windspeed in the CAS (u_c) is given by:

$$u_c = \min\left[0.02, (C_{Dh} u_a)^{1/2}\right] \quad (74)$$

The aerodynamic resistance ($r_{a.f}$) from the foliage to the CAS is formulated in terms of a leaf resistance (r_{leaf}):

$$r_{a.f} = r_{leaf}/(A_L + A_S) \quad (75)$$

$$r_{leaf} = 100(0.04/u_c)^{1/2} \quad (76)$$

The aerodynamic resistance ($r_{a.g}$) from the ground or snow to the CAS is given by:

$$r_{a.g} = 1/\left[C_{Dh}(A_f u_c + (1 - A_f) u_a)\right] \quad (77)$$

4.1.4. Canopy resistance

BASE uses a 'wet canopy resistance' (r_c^*) to represent the influence on E_{tr} of stomatal stresses other than moisture stress and r_c^* is parameterised in terms of minimum canopy resistance ($r_{c.min}$) and stress functions for radiation (f_R), temperature (f_T) and humidity (f_H):

$$r_c^* = \min(r_{c.max}, r_{c.min} f_R f_T f_H) \quad (78)$$

$$f_R^{-1} = R_{s.sa}/200 \quad (79)$$

$$f_T^{-1} = 1 - [(298 - T_f)/25]^2 \quad (80)$$

$$f_H^{-1} = 3 \times 10^{-3}/(q_f^* - q_c) \quad (81)$$

Currently, $r_{c.min}$ is calculated from minimum stomatal resistance (200 s m^{-1}) as:

$$r_{c.min} = (A_L + A_S) r_{s.min} \quad (82)$$

Each of the stress functions is constrained to lie between 0 and 1 and r_c^* is bounded by $r_{c.min}$ and $r_{c.max}$ (5000 s m^{-1}). This general approach follows from Jarvis (1976) and the environmental stress

functions are similar to those used by other LSMs such as BATS and CLASS (Verseghy et al., 1993).

4.2. Subsurface parameters

4.2.1. Physical properties

Physical and geometric soil properties in BASE are characterised by layer thicknesses, root biomass fractions, a soil texture index and a soil colour index.

The thickness of the surface layer (d_1) is always 10 cm and its root fraction (R_1) varies between 50 and 90%, depending on the vegetation type. The second soil layer contains the remainder of the roots (R_2) and its thickness (d_2) is a function of vegetation type. The thickness of the third soil layer (d_3) is set so that the total soil column is always 5 m.

Soil texture (I_{tex}) and colour (I_{col}) indices are developed from the Wilson and Henderson-Sellers (1985) global data-set. I_{tex} varies between 1 for an average sandy soil to 9 for an average clay soil. Values of 1, 5 and 9 are assigned to the coarse, medium and fine soil classes in Wilson and Henderson-Sellers and area-weighting is used to obtain an effective soil texture index for the gridsquare. I_{col} varies from 0 to 1 as soil colour varies from dark to light.

4.2.2. Hydraulic soil properties

The soil's moisture diffusion properties are parameterised in BASE as functions of soil texture (I_{tex}, Section 4.2.1). Cosby et al. (1984) divided 1448 soil samples into eleven texture categories and calculated averages and standard deviations for soil diffusion parameters in each category. In BASE, these eleven soil categories are divided into fine, medium and coarse groups and weighted average parameters are calculated for each group. Following Cosby et al. (1984), a log average is used for K_H^*. Functional relationships between the soil diffusion parameters and I_{tex} are constructed:

$$K_H^* = 10^{-6}(6.9 - 0.64 I_{tex}) \quad (83)$$

$$B = 4 + 0.875(I_{tex} - 1) \quad (84)$$

$$\theta^* = \min[0.45, 0.388 + 0.0125 I_{tex}] \quad (85)$$

There is no consistent relationship between saturated matric potential (Ψ_m^*) and soil texture in Cosby et al. (1984), so BASE uses a single average value of -0.4 m for all soils. In BASE, the extremities of the texture scale are designed to represent average 'fine' and 'coarse' soils rather than very coarse and very fine soils.

Wilting point (θ_{wp}) is specified following Patterson (1990) who calculates average values for fine, medium and coarse-textured soils. A quadratic fit to these values is used in BASE:

$$\theta_{wp} = -1.31 \times 10^{-3} I_{tex}^2 + 0.029 I_{tex} + 0.059 \quad (86)$$

4.2.3. Thermal soil properties

The thermal storage and diffusion properties of the soil in BASE are characterised by heat capacity and thermal conductivity, respectively. These properties are parameterised in terms of the thermal properties of soil components and their volume fractions.

The volumetric heat capacity of a soil layer (C_g, J m^{-3} K^{-1}) is calculated as a weighted average of its components' heat capacities:

$$C_g = \theta C_w + \theta_i C_i + (1 - \theta^*) C_m \quad (87)$$

The volumetric heat capacities for water (C_w, 4.18×10^6 J m^{-3} K^{-1}) and ice (C_i, 1.93×106 J m^{-3} K^{-1}) are obtained from Oke (1987). A typical volumetric heat capacity for the mineral component of the soil (2×10^6 J m^{-3} K^{-1}) is obtained from Hillel (1980). The soil volume occupied by air is considered to have a negligible effect on the overall heat capacity.

Thermal conductivity (K_T, W m^{-1} K^{-1}) in BASE depends on soil texture and moisture content. The parameterisation is constructed around typical conductivities given by Oke (1987) for dry and saturated clay and sandy soils. Following Verseghy (1991), soil moisture saturation fraction is used to linearly interpolate between dry ($K_{T.dry}$) and saturated ($K_{T.sat}$) conductivities:

$$K_T = K_{T.dry} + [(\theta + \theta_i)/\theta^*](K_{T.sat} - K_{T.dry}) \quad (88)$$

$K_{T.dry}$ is expressed as a linear function of BASE's soil texture index (I_{tex}), varying between the sand and clay values given by Oke (1987):

$$K_{T.dry} = 0.25 + [(9 - I_{tex})/8]^* 0.05 \quad (89)$$

The bracketed term in Eq. (89) varies from 0 for an average clay soil to 1 for an average sandy soil. $K_{T.sat}$ is represented by a weighted geometric mean of the constituent conductivities for the water ($K_{T.w}$),

ice ($K_{T.i}$) and mineral ($K_{T.m}$) components of the saturated soil:

$$\log[K_{T.sat}] = \theta/(\theta+\theta_i)\log[K_{T.w}] + \theta_i/(\theta+\theta_i) \times \log[K_{T.i}] + (1-\theta^*)\log[K_{T.m}] \quad (90)$$

$K_{T.m}$ values are selected so that the conductivities of unfrozen saturated clay and sand are equal to the values of Oke (1987). The conductivity for water ($K_{T.w}$) and ice ($K_{T.i}$) are taken from de Vries (1963).

4.3. Snow properties

Snow density (ρ_n, kg m^{-3}) in BASE increases over time as a result of mechanical compaction from overlying snow and decreases when new snow falls. The densification of snow due to self-loading ($d_{\rho n.l}/dt$) is given by:

$$d\rho_{n.l}/dt = 0.5\rho_n g W_n\left[10^{-7}\exp(-0.02\rho_n + 4000/T_n - 14.643)\right] \quad (91)$$

where g is acceleration due to gravity (9.81 m s^{-2}). This expression is based on the work of Kojima (1967) and is discussed in more detail by Cogley et al. (1990) and Slater et al. (1998b). The prognostic snow density variable is updated by volume-weighting old and newly fallen snow:

$$\rho_n^{t+1} = \left[W_n(\rho_n^t + d\rho_{n.l}/dt\Delta t) + 100P_{r.n}\right] /(W_n + P_{r.n}) \quad (92)$$

where ρ_n^t and ρ_n^{t-1} are the old and updated snow densities and Δt is the timestep (s). Fresh snow has a density of 100 kg m^{-3} and the overall snow density is not allowed to exceed 450 kg m^{-3}.

Snowcover fractions for the foliage and ground are parameterised as functions of average snow depth (d_n):

$$A_{ng} = \left[d_n/(0.076 + 0.000288\rho_n)\right]^{1/2} \quad (93)$$

$$A_{nf} = d_n/(d_n + 5z_{0.f}) \quad (94)$$

$$d_n = W_n/\rho_n \quad (95)$$

These A_{nf} and A_{ng} parameterisations follow from BATS and BEST, respectively.

The thermal conductivity of snow ($K_{T.n}$) is expressed as a function of ρ_n following Schwerdtfeger (1963) and Mellor (1977):

$$K_{T.n} = 2.805\times10^{-6}\rho_n^2 \quad (96)$$

Its heat capacity (C_n, J m^{-2} K^{-1}) is given by:

$$C_n = d_n\rho_n C_{p.i} \quad (97)$$

where $C_{p.i}$ is the specific heat capacity of ice (2100 J kg^{-1} K^{-1}; Oke, 1987).

4.4. Land–ice properties

As in BEST, land–ice is parameterised in BASE by altering the standard bare soil parameterisation. Firstly, there are no ice fractions (θ_i) because the 'soil' matrix is composed of ice. The efficiency factor for melting of ice is set to 1. Porosity (θ^*) is set to 0.07. Following Bolsenga (1973), Warren (1982) and Cogley et al. (1990), land–ice albedo is parameterised as a function of θ_1:

$$\alpha = 0.67\left[0.6 + 0.06(1-\theta_1)\right] \quad (98)$$

The heat capacity of the solid 'soil' matrix is set to C_i rather than C_m.

5. Summary

The Best Approximation of Surface Exchange (BASE) land surface model is presented and described in detail. BASE follows from Deardorff (1978) and the BATS and BEST models. It is a full GCM LSM that can be applied to the whole of the global land surface. BASE has participated in both off-line and coupled phases of the Project for Intercomparison of Land-surface Parameterization Schemes (PILPS). BASE is designed principally as an experimental tool for investigating the impact of inter-model parameterisation differences on simulated climate.

Acknowledgements

The work of Deardorff, Dickinson and Cogley in building the framework upon which BASE has been constructed is acknowledged. The efforts of Drew Slater in validation of BASE's snow and frozen soil moisture parameterisations is acknowledged. The contributions of Bryant McAvaney, Dale Hess, Andrea Hahmann and Bertrand Timbal to the coupling of BASE with various atmospheric models is appreciated. This work was performed with the support of an Australian Postgraduate Award.

Appendix A. List of symbols

Symbol**	Meaning	Units
A_{dry}	Heterogeneity parameter for in filtration	–
A_f	Foliage fraction for a surface tile	–
A_n	Ground snow-cover fraction	–
A_{nf}	Foliage snow-cover fraction	–
B	Clapp and Hornberger's soil texture index	–
C_{Dh}	Aerodynamic drag coefficient for heat and moisture	–
$C_{H.sa}$	Aerodynamic transfer coefficient for effective surface	–
C_i	Volumetric heat of water (w), ice (i) or minerals (m)	J m^{-3} K^{-1}
c_p	Specific heat capacity of air	J kg^{-1} s^{-1}
$C_{p.i}$	Specific heat capacity of ice	J kg^{-1} K^{-1}
d_l	Thickness of soil layer l	m
d_n	Average snow depth for whole tile	m
$d_{\rho l}/dt$	Time rate of change in snow density due to self-loading	kg m^{-3} s^{-1}
E	Total evaporation	kg m^{-2} s^{-1}
E_{fc}	Evaporation from foliage interception store	kg m^{-2} s^{-1}
E_g	Direct soil evaporation	kg m^{-2} s^{-1}
$E_{g.sup}$	Maximum supply rate for direct soil evaporation	kg m^{-2} s^{-1}
E_{ij}	Evaporative moisture flux from i to j	kg m^{-2} s^{-1}
E_{tr}	Transpiration	kg m^{-2} s^{-1}
$E_{tr.sup}$	Maximum supply rate for transpiration	kg m^{-2} s^{-1}
f_c	Fractional extent of a surface tile	–
f_f	Foliage fraction	–
f_f^*	Foliage fraction before snowmasking	–
$f_{f.max}$	Maximum foliage fraction parameter	–
$f_{f.seas}$	Foliage seasonality parameter	–
f_H	Stomatal stress factor for humidity [0,1]	–
f_R	Stomatal stress factor for radiation [0,1]	–
f_T	Stomatal stress factor for temperature [0,1]	–
f_{veg}	Total fractional vegetation cover [0,1]	–
f_{wet}	Fraction of foliage covered by water	–
G	Acceleration due to gravity (9.81)	m s^{-2}
G_{ij}	Heat diffusion flux from soil layer i to soil layer j	W m^{-2}
G_{ng}	Heat diffusion flux at base of snowpack	W m^{-2}
H_{ij}	Sensible heat flux from i to j	W m^{-2}
I	Infiltration rate	kg m^{-2}
I^*	Maximum infiltration rate for homogeneous distribution of surface moisture	kg m^{-2}
I_{col}	BASE's soil colour index	–
I_{tex}	BASE's soil texture index	–
K_H^*	Hydraulic conductivity at saturation	–
$K_{H.ij}$	Hydraulic conductivity for fluxes between soil layer i and j	–
$K_{T.dry}$	Thermal conductivity of dry soil	W m^{-1} K^{-1}
$K_{T.i}$	Thermal conductivity within i	W m^{-1} K^{-1}
$K_{T.i}$	Thermal conductivity for water (w), ice (i) and minerals (m)	W m^{-1} K^{-1}
$K_{T.ij}$	Thermal conductivity for fluxes between i and j	W m^{-1} K^{-1}
$K_{T.sat}$	Thermal conductivity of saturated soil	W m^{-1} K^{-1}
k_{VK}	Von Karman constant (0.4)	–
L_{ij}	Evaporative energy (latent heat) flux from i to j	W m^{-2}
P	Precipitation rate	kg m^{-2} s^{-1}
P_n	Total snowfall rate	kg m^{-2} s^{-1}
P_r	Total rainfall rate	kg m^{-2} s^{-1}
q_i	Specific humidity	m^3 m^{-3}
q_i^*	Saturated specific humidity corresponding to temperature T_i	m^3 m^{-3}
r_a	Aerodynamic resistance for surface tile	s m^{-1}
$r_{a.f}$	Aerodynamic resistance from foliage to CAS	s m^{-1}
$r_{a.g}$	Aerodynamic resistance from ground to CAS	s m^{-1}
r_c	Canopy resistance (bulk stomatal resistance (see text).	s m^{-1}

r_c^*	Non-moisture-stressed canopy resistance (see text).	s m^{-1}
$r_{c.max}$	Maximum canopy resistance	s m^{-1}
$r_{c.min}$	Minimum canopy resistance	s m^{-1}
R_{iB}	Bulk Richardson number	–
R_l	Fraction of total root biomass contained in soil layer l	–
$R_{l.ij}$	Longwave radiation flux from i to j	W m^{-2}
$R^*_{l.ij}$	Net longwave radiation flux from i to j	W m^{-2}
r_{leaf}	Aerodynamic resistance for a leaf	s m^{-1}
r_s	Stomatal resistance for a leaf	s m^{-1}
$R_{s.ij}$	Shortwave radiation flux from i to j	W m^{-2}
$R^*_{s.ij}$	Net shortwave radiation flux from i to j	W m^{-2}
$r_{s.min}$	Minimum stomatal resistance	s m^{-1}
R^*	Net radiation	W m^{-2}
S	Seasonality function, S[T]	–
T_I	Temperature	K
T_{rad}	Radiating temperature	K
u_a	Windspeed at atmospheric reference level	m s^{-1}
u_c	Windspeed in canopy air space	m s^{-1}
V_l	Soil moisture saturation fraction in layer l relative to ice-free pore space	m^3 m^{-3}
W_f	Foliage moisture content	kg m^{-2}
$W_{f.max}$	Foliage interception capacity	kg m^{-2}
W_n	Snowpack moisture content	kg m^{-2}
Y_d	Drainage from base of soil column	kg m^{-2} s^{-1}
Y_{ij}	Liquid moisture flux from i to j with numerical indices to indicate soil layers	kg m^{-2} s^{-1}
Y_s	Surface runoff	kg m^{-2} s^{-1}
Z	Root-zone depth	m
$z_{0.c}$	Aerodynamic roughness length for a surface tile	–
$z_{0.i}$	Aerodynamic roughness length for i	–
z_a	Height of atmospheric reference level	m
Δ_t	Model timestep	s
Λ_L	Leaf area index	–
$\Lambda_{L.max}$	Maximum leaf area index parameter	–
$\Lambda_{L.max}$	Leaf area index seasonality parameter	–
Λ_S	Stem area index	–
α_l	Shortwave albedo	–
β_s	Effective surface wetness parameter for BASE s Esa flux	–
λ_i	Latent heat of vaporisation (λ_v), fusion (λ_f) or sublimaiton (λ_s)	J kg^{-1}
θ^*	Porosity	m^3 m^{-3}
θ_{il}	Soil ice saturation fraction in layer l relative to porosity	m^3 m^{-3}
θ_l	Soil moisture saturation fraction in layer l relative to porosity	m^3 m^{-3}
θ_r	Soil moisture saturation fraction in root-zone	m^3 m^{-3}
θ_{wp}	Soil moisture saturation fraction at wilting point	m^3 m^{-3}
ρ_a	Density of air	kg m^{-3}
ρ_n	Density of snowpack	kg m^{-3}
ρ_w	Density of liquid water	kg m^{-3}
σ_{sb}	Stefan–Boltzmann constant ($5.67 \times 10-8$)	W m^{-2} K^{-4}
λ_l	Efficiency factor for melting/freezing of soil moisture in layer l	–
Ψ_l	Moisture potential in soil layer l	m
Γ_l	Flux of moisture due to freezing/melting in layer l	kg m^{-2} s^{-1}
Ψ_m	Matric potential	m
Ψ_m^*	Matric potential at saturation	m
Ψ_{wp}	Moisture potential at wilting point	m

** Italicised indices i, j and l are used to represent families of symbols. They can represent the atmosphere (a), surface (s), canopy air space (c), foliage (f), ground (g), snow (n), upper soil layer (g1), middle soil layer (g2) or lower soil layer (g3). The indices may be left blank to indicate a more general reference.

References

Abramopoulos, F., Rosenzweig, C.E., Choudhury, B., 1988. Improved ground hydrology calculations for global climate models (GCMs): soil water movement and evapotranspiration. J. Climate 1, 921–941.

Acker, T., Buja, L.E., Rosinski, J.M., Truesdale, J.E., 1996. User's Guide to NCAR CCM3. NCAR tech. note NCAR/TN-421+IA, Boulder, CO, 210 pp.

Bolsenga, S.J., 1973. Preliminary observations on the daily variations of ice albedo. J. Glaciol. 18, 517–521.

Bonan, G.B., 1994. Comparison of two land surface process models using prescribed forcings. J. Geophys. Res. 99, 25803–25818.

Bonan, G.B., 1996. A land surface model (LSM version 1.0) for ecological, hydrological, and atmospheric studies: technical description and user's guide. NCAR tech. note, TN-417+STR, 150 pp.

Budyko, M.I., 1956. The heat balance of the earth's surface. Gidrometeoizdat, Leningrad.

Chen, T.H., Henderson-Sellers, A., Milly, P.C.D., Pitman, A.J.,

Beljaars, A.C.M., Polcher, J., Abramopoulos, F., Boone, A., Chang, S., Chen, F., Dai, Y., Desborough, C.E., Dickinson, R.E., Dumenil, L., Ek, M., Garratt, J.R., Gedney, N., Gusev, Y.M., Kim, J., Koster, R., Kowalczyk, E.A., Laval, K., Lean, J., Lettenmaier, D., Liang, X., Mahfouf, J.-F., Mengelkamp, H.-T., Mitchell, K., Nasonova, O.N., Noilhan, J., Polcher, J., Robock, A., Rosenzweig, C., Schaake, J., Schlosser, C.A., Schulz, J.-P., Shmakin, A.B., Verseghy, D.L., Wetzel, P., Wood, E.F., Xue, Y., Yang, Z.-L., Zeng, Q., 1997. Cabauw experimental results from the project for intercomparison of landsurface parameterization schemes. J. Climate 10, 1144–1215.

Clapp, R.B., Hornberger, G.M., 1978. Empirical equations for some soil hydraulic properties. Water Resour. Res. 14, 601–604.

Cogley, J.G., Pitman, A.J., Henderson-Sellers, A., 1990. A land surface for large scale climate models. Trent University technical note 901, Trent University, Peterborough, Ontario, K9J 7B8, Canada, 129 pp.

Cosby, B.J., Horberger, G.M., Clapp, R.B., Ginn, T.R., 1984. A statistical exploration of the relationships of soil moisture characteristics to the physical properties of soils. Water Resour. Res. 20, 682–690.

de Vries, D.A., 1963. Thermal properties of soils. In: Van Wijk, W.R. (Ed.), Physics of Plant Environment. North-Holland, 595 pp.

Deardorff, J.W., 1978. Efficient prediction of ground surface temperature and moisture, with inclusion of a layer of vegetation. J. Geophys. Res. 83, 1889–1903.

Desborough, C.E., 1997. Impact of root-weighting on the response of transpiration to moisture stress in land surface schemes. Mon. Weather Rev. 125, 1920–1930.

Dickinson, R.E., Henderson-Sellers, A., Kennedy, P.J., Wilson, M.F., 1986. Biosphere atmosphere transfer scheme (BATS) for the NCAR community climate model. NCAR tech. note TN275+STR, National Center for Atmospheric Research, Boulder, CO, 69 pp.

Ducoudre, N.I., Laval, K., Perrier, A., 1993. SECHIBA: a new set of parameterizations of the hydrologic exchanges at the land–atmosphere interface within the LMD atmospheric general circulation model. J. Climate 6, 248–273.

Henderson-Sellers, A., Yang, Z.-L., Dickinson, R.E., 1993. The project for intercomparison of land-surface parameterisation schemes. Bull. Am. Meteorol. Soc. 74, 1335–1349.

Henderson-Sellers, A., Pitman, A.J., Love, P.K., Irranejad, P., Chen, T.H., 1995. The project for intercomparison of land-surface parameterisation schemes (PILPS): phases 2 and 3. Bull. Am. Meteorol. Soc. 76, 489–503.

Henderson-Sellers, A., McGuffie, K., Pitman, A.J., 1996. The project for intercomparison of land-surface parameterization schemes (PILPS): 1992 to 1995. Climate Dynamics 12, 849–859.

Hess, G.D., McAvaney, B.J., 1997. Note on computing screen temperatures, humidities and anenometer-height winds in large-scale models. Aust. Meteorol. Mag. 46, 109–115.

Hillel, D., 1980. Fundamentals of Soil Physics. Academic Press, New York.

Jarvis, P.G., 1976. The interpretation of the variations in leaf water potential and stomatal conductance found in canopies in the field. Philos. Trans. R. Soc. London, Ser. B 273, 593–610.

Kim, J., Ek, M., 1995. A simulation of the surface energy budget and soil water content over the hydrologic atmospheric pilot experiments—modelisation du Bilan Hydrique forest site. J. Geophys. Res. 10, 20845–20854.

Kojima, K., 1967. Densification of seasonal snow cover. Physics of snow and ice. Proc. Int. Conf. Low Temp. Sci. 1, 929–952.

Koster, R.D., Milly, P.C.D., 1997. The interplay between transpiration and runoff formulations in land surface schemes used with atmospheric models. J. Climate 10, 1578–1591.

Koster, R.D., Suarez, M.J., 1992. Modelling the land surface boundary in climate models as a composite of independent vegetation stands. J. Geophys. Res. 97, 2697–2715.

Kowalczyk, E.A., Garratt, J.R., Krummel, P.B., 1991. A soil-canopy scheme for use in a numerical model of the atmosphere-1D stand-alone model. CSIRO Division of Atmospheric research technical paper no. 23.

Mahfouf, J.-F., Manzi, A.O., Noilhan, J., Giordani, H., Deque, M., 1995. The land surface scheme ISBA within the meteo-France climate model ARPEGE: Part I. Implementation and preliminary results. J. Climate 8, 2039–2057.

Manabe, S., 1969. Climate and the ocean circulation: 1. The atmospheric circulation and the hydrology of the earth's surface. Mon. Weather Rev. 97, 739–805.

McAvaney, B.J., Colman, R.A., 1993. The AMIP experiment: The BMRC AGCM configuration. BMRC research report no. 38, Bureau of Meteorology Research Centre, Melbourne, Australia, 43 pp.

McAvaney, B.J., Fraser, J.R., Hart, T.L., Rikus, L.J., Bourke, W.P., Naughton, M.J., Mullenmeister, P., 1991. Circulation statistics from a non-diurnal seasonal simulation with the BMRC atmospheric GCM: R21L9. BMRC research report no. 29, Bureau of Meteorology Research Centre, Melbourne, Australia, 231 pp.

Mellor, M., 1977. Engineering properties of snow. J. Glaciol. 19, 15–66.

Monteith J.L., 1965. Evaporation and environment. In: Fogg, G.E. (Ed.), The State and Movement of Water in Living Organisms. Cambridge Univ. Press, Cambridge, pp. 205–234.

Noilhan, J., Planton, S., 1989. A simple parameterization of land surface processes for meteorological models. Mon. Weather Rev. 117, 536–549.

Oke, T.R., 1987. Boundary Layer Climates. Routledge, London.

Patterson, K.A., 1990. Global distributions of total and total-available soil water-holding capacities. MSc thesis, University of Delaware, 119 pp.

Penman, H.L., 1948. Natural evaporation from open water, bare soil and grass. Proc. R. Soc., Ser. A 193, 120–145.

Pitman, A.J., Desborough, C.E., 1996. Brief description of bare essentials of surface transfer and results from simulations with the HAPEX-MOBILHY data. Global Plan. 13, 135–143.

Pitman, A.J., Henderson-Sellers, A., 1997. Recent progress and results from the project for intercomparison of landsurface parameterization schemes. Submitted to J. Hydrol.

Pitman, A.J., Yang, Z.-L., Cogley, J.G., Henderson-Sellers, A.,

1991. Description of Bare Essentials of Surface Transfer for the Bureau of Meteorology Research Centre AGCM. BMRC research report, 32, Melbourne, Australia, May, 1991.

Pitman, A.J., Henderson-Sellers, A., Abramopoulos, F., Boone, A., Desborough, C.E., Dickinson, R.E., Garratt, J.R., Gedney, N., Hahmann, A., Koster, R., Kowalczyk, E., Laval, K., Lettenmaier, D., Liang, X., Mahfouf, J.-F., Noilhan, J., Polcher, J., Qu, W., Robock, A., Rosenzweig, C., Schlosser, C.A., Shmakin, A.B., Smith, J., Suarez, M., Verseghy, D., Wetzel, P., Wood, E., Xue, Y., Yang, Z.-L., 1998. Results from the off-line control simulation phase 1c of the Project for Intercomparison of Land-surface Parameterization Schemes (PILPS). Submitted to Climate Dynamics.

Pollard, D., Thompson, S.L., 1995. Use of a land-surface-transfer scheme (LSX) in a global climate model: the response to doubling stomatal resistance. Global Plan. 10, 129–161.

Schwerdtfeger, P., 1963. Theoretical derivation of the thermal conductivity and diffusivity of snow. Insl. Assoc. Sci. Hydrol. Publ. 61, 75–81.

Sellers, P.J., Mintz, Y., Sud, Y.C., Dalcher, A., 1986. A simple biosphere model (SiB) for use within general circulation models. J. Atmos. Sci. 43, 503–531.

Slater, A.G., Pitman, A.J., Desborough, C.E., 1998a. The simulation of freeze–thaw cycles in a GCM land surface parameterization scheme. Accepted by J. Geophys. Res. (Atmos.).

Slater, A.G., Pitman, A.J., Desborough, C.E., 1998b. The validation of a snow parameterization designed for use in general circulation models. Accepted by Int. J. Climatol.

Timbal, B., Henderson-Sellers, A., 1998 Intercomparisons of land-surface parameterisations coupled to a limited area forecast model. Accepted by Global and Planetary Change.

Verseghy, D.L., 1991. CLASS: a Canadian land surface scheme for GCMs. I. Soil model. Int. J. Climatol. 11, 111–133.

Verseghy, D.L., McFarlane, N.A., Lazare, M., 1993. CLASS—a Canadian land surface scheme for GCMs. II: Vegetation model and coupled runs. Int. J. Climatol. 13, 347–370.

Viterbo, P., Beljaars, A.C.M., 1995. An improved land surface parameterization scheme in the ECMWF model and its validation. J. Climate 8, 2716–2748.

Warren, S.G., 1982. Optical properties of snow. Rev. Geophys. 20, 67–89.

Wilson, M.F., Henderson-Sellers, A., 1985. A global archive of land cover and soil data sets for use in general circulation climate models. J. Climatol. 5, 119–143.

Xue, Y., Sellers, P.J., Kinter, J.L., Shukla, J., 1991. A simplified biosphere model for climate studies. J. Climate 4, 345–364.